Ad Hoc Networks 107 (2020) 102226

Contents lists available at ScienceDirect

Ad Hoc Networks

journal homepage: www.elsevier.com/locate/adhoc

WiRelax: Towards real-time respiratory biofeedback during meditation using WiFi

Abdelwahed Khamis, Research Associate[a,*], Brano Kusy, Principal Research Scientist[b], Chun Tung Chou, Associate Professor[a], Wen Hu, Associate Professor[a]

[a] UNSW, High Street, Kensington, NSW 2033, Sydney, Australia
[b] Queensland Centre for Advanced Technologies, Pullenvale, QLD 4069, Australia

ARTICLE INFO

Article history:
Received 14 September 2019
Accepted 27 May 2020
Available online 7 June 2020

Keywords:
Biofeedback
Breathing
WiFi
Device-free

ABSTRACT

Respiratory pattern tracking proved to be critical for many applications ranging from well-being monitoring and stress management to dealing with chronic breathing abnormalities. Specific breathing and meditation exercises have been designed to improve well-being of users based on monitoring the **complete breathing waveform**. While wearable systems had leveraged a wealth of information available from respiration stream in a variety of applications, contact-less sensing systems are lagging behind when it comes to capturing detailed breathing metrics. In this work we propose WiRelax; the first non-contact respiratory biofeedback system that relies solely on WiFi availability. We propose algorithms that map the changes in the Channel State Information (CSI) to the instantaneous breathing state. The key contribution is a model that relates relative phase of the received signal and the micro-motion of the chest during breathing. A novel processing pipeline is developed to extract a single breathing waveform from CSI data captured across noisy multiple sub-carriers in real-time. Our evaluation in a real-world setup shows that WiRelax can estimate real-time breath-by-breath cycle time with median error less than 0.25 s ($<$ 13% relative to the cycle length) thus enabling accurate device-free respiratory biofeedback.

© 2020 Elsevier B.V. All rights reserved.

1. Introduction

Awareness of one's breathing habits and conscious breathing techniques leads to reduced stress and is considered fundamental to achieving physical and mental well-being. Detailed respiratory pattern information is highly discriminatory of physiological stress [1]. Additionally, breathing exercises are frequently used in clinical treatment of breathing related disorders such as Attention Deficit Hyperactivity Disorder (ADHD), Chronic Obstructive Pulmonary Disease (COPD) and Asthma [2–4].

Real-time access to fine-grained breathing data and the assessment of a subject's breathing quality are crucial tools used across these applications. Monitoring of breathing is most commonly achieved with ***dedicated wearables*** that users wear during an exercise, including textile sensors, wearable belts, or sensors attached to the chest [5–7]. Several commercial products use wearable technology to assess respiratory patterns. For example, Spire [8] monitors user stress based on breathing features such as rate, depth, inhalation-to-exhalation ratio (IER), durations of inhalation and coaches the user towards calmer breathing to alleviate the stress. Similarly, Prana [9] monitors depth, retention, smoothness, exhalation time, and time between breaths [9] and allows users to pick from a library of breathing exercises such as Yoga Pranayama, Tai Chi, and Buteyko for retraining their breathing patterns. In addition to dedicated wearables, increasing number of smartphone apps target the space of meditation and breathing exercises. Smartwatch manufacturers are already integrating mindfulness software in their products. For example, Apple's Breathe app [10] guides the user during breathing exercises by requiring him to breathe-in/out following a circle animation. However, this is done without actual monitoring of the breathing progress. Such guidance is blind to subject behavior and lacks continuous feedback

On the other hand, ***Device-free systems*** provide a more comfortable alternative, especially when monitoring is required over long-term. Majority of device-free systems use wireless radio signals and relatively expensive hardware to monitor user breathing, including FMCW radar [12], USRP [13] or Doppler radar [14], which ***limits their deployment potential***. Off-the-shelf WiFi technology provides a viable cost-effective alternative [15–17]. However, existing WiFi-based systems primarily focus ***on breathing rate*** estimation and cannot report detailed instantaneous respiratory pattern

* Corresponding author.
E-mail addresses: a.khamiss@unsw.edu.au (A. Khamis), Brano.Kusy@data61.csiro.au (B. Kusy), c.t.chou@unsw.edu.au (C.T. Chou), wen.hu@unsw.edu.au (W. Hu).

https://doi.org/10.1016/j.adhoc.2020.102226
1570-8705/© 2020 Elsevier B.V. All rights reserved.

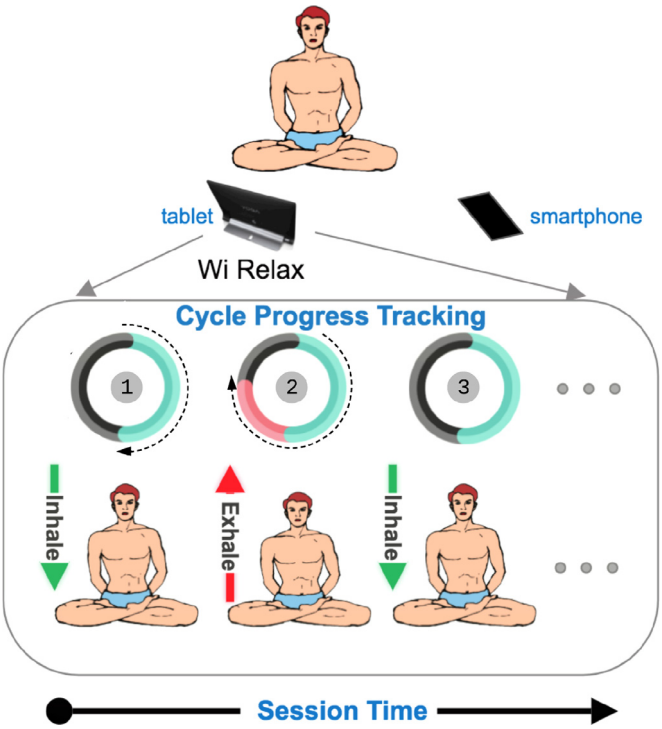

Fig. 1. WiRelax leverages WiFi communication to provide subject with Instantaneous respiratory feedback during meditation sessions (demo: [11]).

information. Questions about the ongoing respiratory pattern, such as, current cycle (inhalation/exhalation/retention), timing (e.g. inhaling for 0.75 s), breathing depth (e.g. shallow/deep) can't be answered directly using existing approaches. These information are equally important in biofeedback and well-being monitoring applications and ***ubiquitous contact-free breathing biofeedback solution is yet to be realized***.

In this paper we propose ***WiRelax***, a device-free system for real-time monitoring of detailed breathing patterns of a user, which is a key enabler of breathing exercise and biofeedback systems. The system is based on analyzing channel state information (CSI) of WiFi packets transmitted between two commodity WiFi devices, such as a tablet and a smartphone (see Fig. 1).

WiRelax needs to inform the subject about the instantaneous breathing performance (duration and depth) within the breathing session. Instantaneous reporting provides timely feedback and enables the subject to apply breath control action. Consider the scenario illustrated in Fig. 1 in which the subject is practicing 6-second paced breathing (3 s inhalation & 3 s exhalation). The visual feedback consists of a color-coded circle that progresses in the direction of the dashed arrow as the system senses user inhaling (green color) and exhaling (red color). In state 2, for example, the subject observes that he completed 50% of the exhalation cycle and has 1.5 s more to go (gray segment). Ultimately, instantaneous sensing and feedback allow him to synchronize his breathing with the desired exercise settings.

Several challenges arise in our use-case scenario. First, we require the breathing progress to be reported continuously during the breathing cycle. Conventional peak-to-peak distance [16] and frequency analysis [15,18] approaches that are used to estimate breathing rate are unsuitable for this purpose as their estimates are performed on completed cycles segments (Fig. 2). We address the challenge by introducing a model that correlates the instantaneous breathing-induced chest displacement of the user to the change in CSI properties of the WiFi signal sub-carriers. According to the model, the chest displacement will cause a linear shift in the

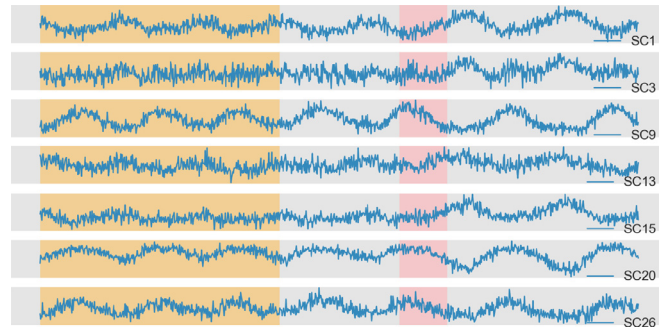

Fig. 2. Cycle counting vs. instantaneous breath tracking: most CSI streams agree on breath cycles count (3 cycles in orange segment), but they lack consensus about instantaneous breath (i.e. whether the subject is inhaling or exhaling and at what depth in the red segment). WiRelax addresses instantaneous breath tracking. (For interpretation of the references to colour in this figure legend, the reader is referred to the web version of this article.)

receiver antennas phase difference. Additionally, the shift is proportional to the chest displacement magnitude, which enables us to identify breathing depth (shallow vs deep breathing). Driven by the model, a novel signal processing pipeline is developed to address the practical considerations of filtering out noisy sub-carriers and fusing streams from many sub-carriers into a single breathing waveform.

Our second challenge is the requirement to distinguish inhalation and exhalation cycles, as it has been shown that Inhalation/Exhalation Ratio (IER) modulates heart rate variability [19]. Reporting IER and other similar metrics is contingent on the ability to make such distinction. We solve this problem through a calibration procedure in which we ask the user to perform a pre-specified breathing sequence at the beginning of the session. The calibration takes few seconds and makes the system agnostic to environmental changes and subject identities

Ultimately, the estimated waveform accurately matches the timing of the inhalation/exhalation cycles and the amplitude of the chest displacement. Our results in Section 4 show that the timing errors are less than 0.5 s 83% of the time and the correlation between estimated breathing waveform and the ground truth is 77%.

Our contributions are summarized as follows:

1. We propose the first WiFi-based contact-less real-time monitoring system for ongoing breathing cycles.
2. We model the relationship between breathing-related chest displacement and the change in phase difference (PD) of commodity WiFi packets. Unlike earlier models [15,20] that focus on breathing frequency, the proposed model is designed to infer instantaneous breathing dynamics (timing and depth) making it suitable for biofeedback applications.
3. We demonstrate the effectiveness of the system by capturing detailed breathing pattern metrics in real-world trials. Specifically, we capture inhalation time, exhalation time, and relative amplitude, and inhalation-to-exhalation ratio (IER).

The rest of the paper is organized as follows. Section 2 presents an overview of the proposed WiRelax system which can accurately capture the chest displacement profile of subjects. We then present an analytical model that captures how chest displacement affects the antenna phase difference in Section 3. This section also describes the algorithm WiRelax uses to process the CSI data. Section 4 evaluates the performance of WiRelax, Section 5 discusses related work. Section 6 discusses limitations and future directions and Section 7 concludes the paper.

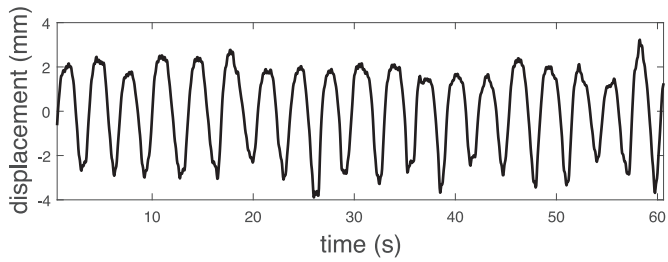

Fig. 3. A sample breathing session.

2. Overview

In this section, we motivate our work using an illustrative example and provide a brief overview of WiRelax. Detailed description of the system will be presented in the next section.

2.1. Motivating example

Our objective is to develop a system for real-time monitoring of detailed breathing dynamics of a user. Our key insights are best illustrated through an example. We conducted an experiment with a single subject and two contact-less systems in a closed room. We used a UWB radar[1] to capture the ground truth data for the chest movement (plotted in Fig. 3). We also deployed two laptops, one transmitter and one receiver, to measure CSI data using an Intel 5300 WiFi card. We processed the CSI data using the procedure in [16], where for each sub-carrier, a Hampel filter was applied to remove outliers and then a moving average filter was used to remove the high frequency noise irrelevant to breathing.

We plot the amplitude of the processed CSI data across sub-carriers and phase difference of the CSI data between the two receiver antennas in Fig. 4. The top part of sub figures show the data for all sub-carriers, while the bottom sub-figures show the sub-carrier with the highest variance[2]. The ground-truth breathing waveform is shown in Fig. 3.

We observe that while the frequency of the oscillation of the breathing waveform is preserved in both the amplitude and phase of the CSI data, the amplitude of the breathing waveform (the chest displacement in Fig. 3) does not correlate well with the CSI amplitude. Phase difference, on the other hand, shows a high correlation with the breathing waveform and is more suitable for monitoring breathing patterns with a fine-grained detail. Based on this observation our modelling is based on phase difference measurements. Next, we give overview of how the system works then, in Section 2, we introduce the model and system implementation.

2.2. WiRelax overview

WiRelax works by tracking a stationary user that is seated in a room equipped with two devices with commodity WiFi. At least one of the devices has multiple antennas, which is a common hardware feature used to improve spatial diversity of WiFi communications.

Our system works in two steps. First, the user is asked to inhale and exhale normally for 10 s to calibrate the system. The calibration step generates a user model that links the RF signal to user's breathing. Next, the system provides the user with detailed information about his breathing patterns in real-time, through the conscious breathing graphical user interface (prototype in Fig. 13)

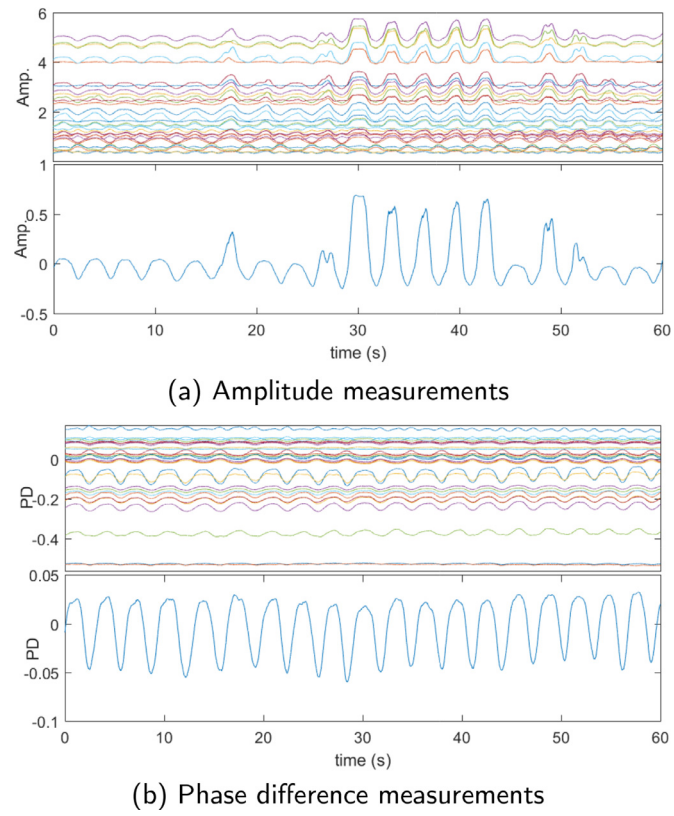

Fig. 4. Recorded amplitude and phase difference for the breathing signal of Fig. 3.

Fig. 5 shows the key algorithmic steps. The system first captures CSI data for both receiver antennas and calculates phase difference (PD) between the two CSI streams, referred to as *Raw PD*. The raw data is then preprocessed to remove noise present in all sub-carriers. Next, the system rejects outlier sub-carriers and selects one of the remaining sub-carriers as a "reference" in the *Selection and Alignment* step. In this stage, sub-carriers that have the opposite phase of the reference are inverted to be aligned. In the *Waveform Estimation* step, the data across all of the sub-carriers is fused into a single CSI waveform, using linear regression. Finally, the user model from the calibration step is used to transform the CSI waveform to the breathing waveform.

3. WiRelax system

In this section, we discuss the implementation of WiRelax. We start by modeling the relationship between chest displacement and antennas phase difference of the radio signals. We then present our pre-processing steps to de-noise the signals and a data fusion algorithm for combining data from multiple sub-carriers into a single breathing waveform.

3.1. The impact of chest displacement on sub-carrier phase difference

This section gives the intuition on how displacement affects the phase difference of the CSI. A more detailed mathematical analysis will be provided in Section 3.2.

WiRelax works with two receiver antennas, and we will use the term *phase difference* (PD) to refer to the phase difference measured between the two antennas, typically calculated using the received CSI data. The term should not be confused with *path phase difference* commonly found in the literature, which refers to the

[1] Xethru X2-M200 radar (https://novelda.com/)

[2] A sub-carrier's variance is an indicator of its sensitivity [16]

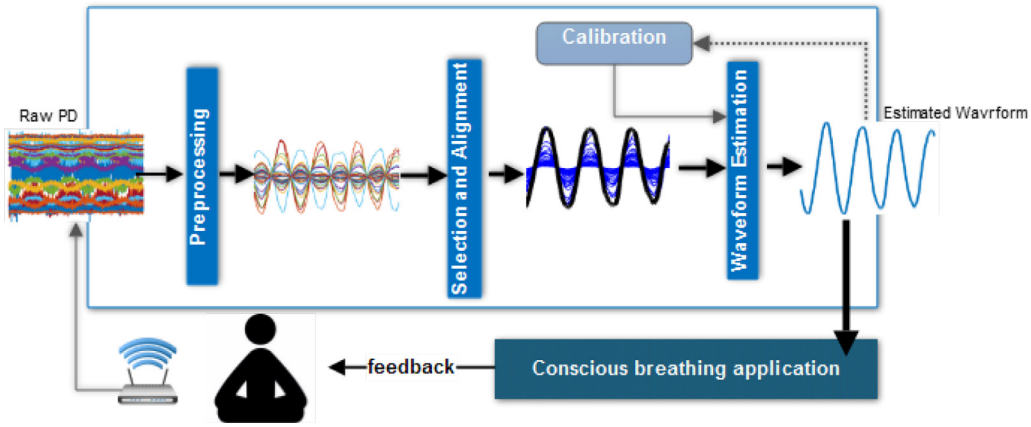

Fig. 5. Illustration of WiRelax architecture. WiRelax is meant to be a framework that supports conscious breathing applications by providing real-time detailed breathing waveform.

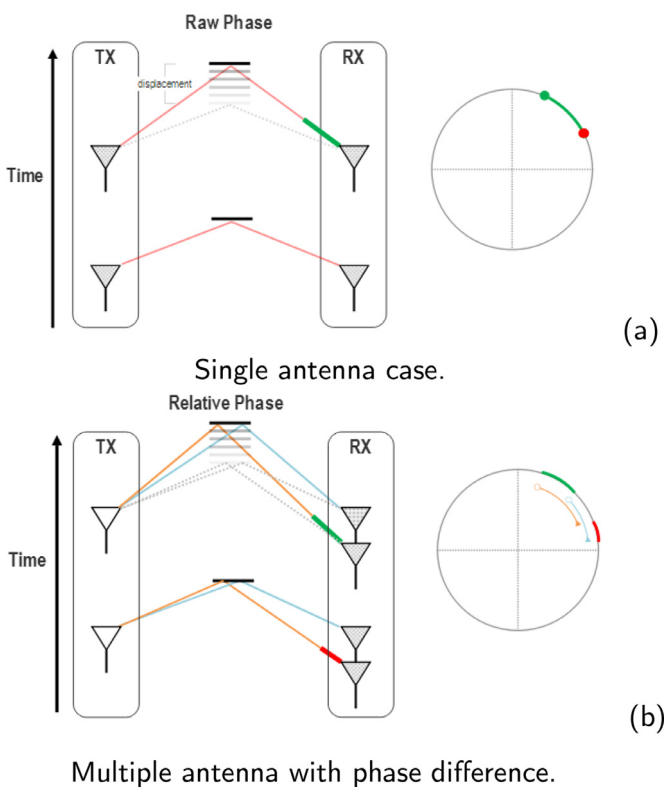

Fig. 6. The effect of object displacement on phase.

phase difference between two signals (typically direct path and a reflection) as recorded by a single receiver antenna [20,21]. The latter cannot be measured from COTS WiFi but its impact on the received CSI amplitude was modeled by earlier efforts and employed in various applications [15,21].

We consider the situation in Fig. 6(a) where a transmitter (TX), a receiver (RX) and a slowly-moving reflector (depicted as a thick horizontal line) are lying on a plane. We assume that the reflector moves in the direction perpendicular to the line connecting the transmitter and receiver. We consider ray tracing and in particular the ray from transmitter to receiver via the reflector. We see from Fig. 6(a) that the movement of the reflector causes the length of this ray to extend. In particular, the thick green line shows the extra path traversed by the signal compared with an earlier time instance. This extra path length $\Delta\ell$ causes an extra phase shift $\Delta\phi$ at the receiver [12]:

$$\Delta\phi = 2\pi\frac{\Delta\ell}{\lambda} \tag{1}$$

where λ denotes the wavelength. Since the extra path length $\Delta\ell$ is related to displacement of the reflector, the extra phase shift $\Delta\phi$ therefore contains information on the unknown displacement. This method of estimating displacement from phase shift has been employed in [12,22]. However, this method requires the transmitter and the receiver synchronise their radio carriers, which is not available for commodity WiFi. In this paper, we will overcome the lack of carrier synchronisation in WiFi by using the phase difference between two antennas of the same receiver.

Consider the situation in Fig. 6(b), which is similar to that of Fig. 6(a), except that the receiver has two antennas. We again consider ray tracing. There is a reflected ray from the transmitter to each of the two antennas, shown as thin blue and orange lines. The orange ray travels over a longer path length and the path length difference between the two rays are shown as thick red line (lower part of the figure) and thick green line (upper part of the figure). The extra path causes a phase difference between the received signals at the two receiver antennas and we use it to estimate the displacement of the reflector.

Note that the phase difference is computed with respect to a common transmitter antenna which acts as a reference. Therefore, the lack of synchronisation between the transmitter and receiver is not a concern. Also, we assume that the unknown displacement that we want to measure is small enough so that the extra path length is less than one wavelength. This allows our system to be agnostic to the phase wrap-around problem, where many different extra path lengths correspond to the same phase difference (e.g. a phase difference of $\frac{\pi}{2}$ can be due to extra path lengths of $\frac{\lambda}{4}$, $\lambda+\frac{\lambda}{4}$, $2\lambda+\frac{\lambda}{4}$ etc). In our scenario, the expected movement of the chest is in the range of 4–12 mm and the wavelength of the 5GHz signals is 5.7 cm [15].

3.2. Modeling the impact of displacement on phase difference

The aim of this section is to derive a mathematical expression relating the phase difference between two receiver antennas as a function of the displacement of the chest as a reflector. We consider the situation depicted in Fig. 7, which has the same setup as that in Fig. 6(b) but with relevant distance labeled to facilitate the mathematical analysis. Table 1 summarises the symbols used in the mathematical analysis.

Table 1
Symbols used in the mathematical derivation.

Symbol	Description
d	Distance between TX and RX in the x-direction
k	Distance between the two receiving antennas
h_t	Nominal distance between the transmitting and the reflector in the y-direction
h_r	Distance between the receiving antenna 1 and the reflector in the y-direction
ϵ	Displacement of the reflector in the y-direction from the nominal distance

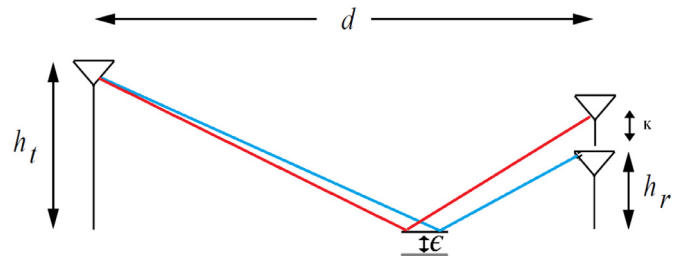

Fig. 7. Illustrative example annotated with key symbols used in the model derivation.

Our model is based on ray tracing. We consider two rays for each antenna: (1) LoS propagation from the transmitting antenna; (2) Reflected ray by the chest. The difference in path length Δp_{LOS} for the two LoS rays reaching the two antennas is:

$$\Delta p_{\text{LOS}} = \sqrt{((h_t - h_r)^2 + d^2} - \sqrt{((h_t - (h_r + k))^2 + d^2} \quad (2)$$

This path length difference is independent of the chest displacement. Without loss of generality, we assume $h_t = h_r = h$. Since the inter-antenna distance k is small compared to d, we assume that Δp_{LOS} is negligible.

When the chest is at a distance of ϵ from its nominal position, the difference in path lengths $\Delta p(\epsilon)$ for the two reflected rays reaching the two antennas is a function of ϵ, as follows:

$$\Delta p(\epsilon) = \sqrt{(h_t + h_r + 2\epsilon)^2 + d^2} - \sqrt{((h_t + (h_r + k) + 2\epsilon)^2 + d^2} \quad (3)$$

This results in a phase difference $\Delta\phi(\epsilon)$ between the two receiving antennas:

$$\Delta\phi(\epsilon) = \frac{2\pi}{\lambda}\Delta p(\epsilon) \quad (4)$$

We again assume that $h_t = h_r = h$. Since the chest displacement ϵ is small compared with h, we approximate the right-hand side of Eq. (3) using the Taylor's series expansion in ϵ that retains only up to linear term. With this approximation, we have:

$$\Delta\phi(\epsilon) - \Delta\phi(0) = \frac{2\pi}{\lambda}\epsilon S \quad (5)$$

where

$$S = \left.\frac{\partial \Delta p(\epsilon)}{\partial \epsilon}\right|_{\epsilon=0} = \frac{4h}{\sqrt{(2h)^2 + d^2}} - \frac{4h + 2k}{\sqrt{(2h + k)^2 + d^2}} \quad (6)$$

We assume that WiFi has C sub-carriers with wavelengths λ_i where $i = 1, \ldots, C$ and for the ith sub-carrier, the measured phase difference between receiver antennas is $\Delta\phi_i(\epsilon)$. By using Eq. (5) for all C sub-carriers, we have:

$$\frac{\Delta\phi_i(\epsilon) - \Delta\phi_i(0)}{2\pi} = \frac{1}{\lambda_i}\epsilon S \quad \text{for } i = 1, \ldots, C. \quad (7)$$

If we perform a linear regression with $\frac{\Delta\phi_i(\epsilon) - \Delta\phi_i(0)}{2\pi}$ as the dependent variable and $\frac{1}{\lambda_i}$'s as the regressors, then the estimated slope is ϵS. We see from Eq. (6) that the constant S depends on the distances between the transmitter, receiver and the user. Although it may be possible to obtain the value of S through some calibration process, this process can be cumbersome. In this paper, we will use the estimated slope to determine the chest displacement up to a proportional constant and we will refer to that as the relative displacement.

3.3. Relative displacement estimation

Our proposed system uses the phase difference between a pair of receiver antennas as the input.

In the beginning, our system acquires and processes phase difference signal for a calibration period of 10 s in which the user is asked to breath normally. A model of the amplitude and phase of user's breathing is kept as a result of this step. Next, the system follows a series of processing steps to remove noise in the CSI samples, reject outlier sub-carrier data, and to fuse data from multiple sub-carriers. Overview of the steps was presented in Fig. 5. We next describe the individual processing steps in a more detail.

3.3.1. Calibration

In the calibration step, the system instructs the user to breathe normally for 10 s and then gives an audio cue to indicate the start of the calibration step. During calibration, the subject is expected to hold the breath for about a second, then repeatedly breath in and breath out in relaxed manner until the end of calibration, signaled with another audio cue. After that, the subject will follow the breathing exercises. The system records CSI data during calibration, which is subsequently used to resolve ambiguity in the sign of $\pm 180^o$ phase shift, which in turn causes ambiguity in distinguishing between inhalation and exhalation. By asking the subject to inhale first before exhaling in the calibration process, we can capture the sign corresponding to inhalation and exhalation for them to be correctly identified later. In summary, the calibration data is used to model:

- **Amplitude of the normal breathing**: The median of the estimated breathing amplitude during calibration is kept as the reference amplitude. The information is used for tracking breathing depth.
- **Direction of the phase difference in Inhalation and Exhalation cycles**: Identifying inhalation vs exhalation is achieved by relating the change in the produced waveform to the actual expected breathing pattern during calibration. The information is vital for capturing inhalation/exhalation ratio among other metrics.

It should be noted that the calibration stage (10 s) is performed **once** in the beginning of each breathing session (lasting 10–15 min).

3.3.2. Denoising and outlier removal

The aim of the preprocessing step is to de-noise the signal before handing it over to the filtering module. The preprocessing is done for each individual sub-carrier independently. First, we use the Hampel filter to remove outlier samples that render themselves

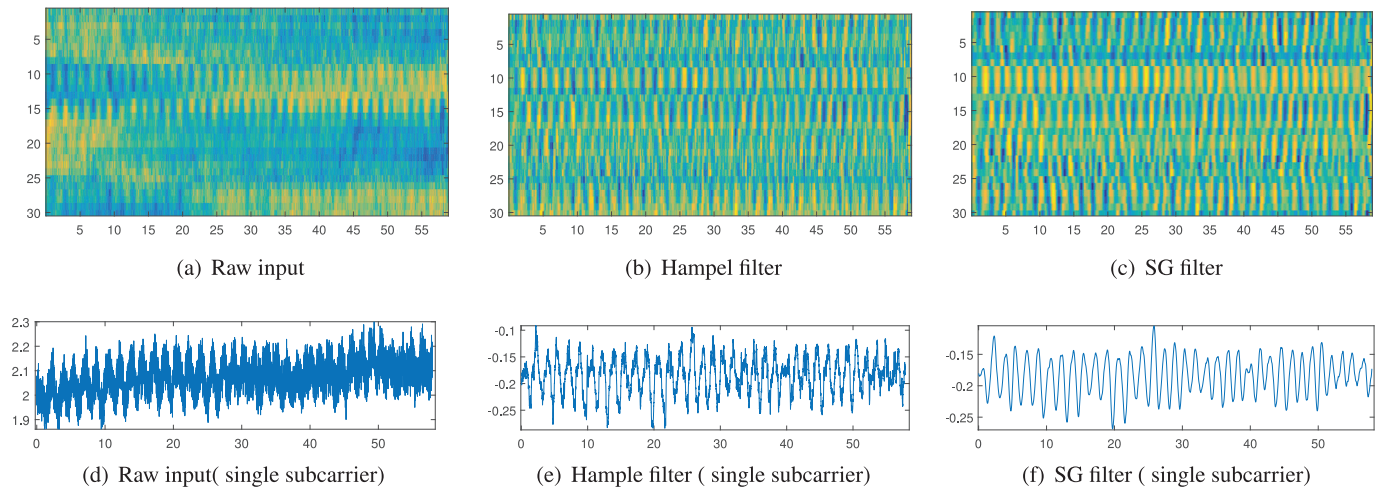

Fig. 8. Preprocessing. Preprocessing depicted for a 1-minute segment of breathing session (rate 40*bpm*). Time is on x-axis. Lower row show preprocessing sequence applied to a single sub-carrier (#9) while upper one depict the preprocessing impact on all sub-carriers (sub-carriers numbers on y-axis). Values in upper sub-figures scaled to range [0–1] for each sub-carrier for visualization purposes.

as abrupt changes. In particular, we discard any point falling outside the range of $[\mu - \tau * \sigma, \mu + \tau * \sigma]$, where μ, σ and τ are the median, mean absolute deviation and the threshold, respectively. The window size is set to 1 s. Next, to filter-out irrelevant high frequency noise, the sub-carriers streams are subjected to a moving average filter. We use a moving average filter with a larger window size (defaulted to 3.5 s) to extract the sub-carrier dynamic trend. We then subtract the obtained trend from the original data stream to get the de-trended data (Fig. 8(e)).

We observed during our experimentation that occasionally a few (typically fewer than 3) noisy sub-carriers are present in the data. These noisy sub-carriers vary in a random way throughout the whole breathing session and do not reflect the actual breathing. Excluding these sub-carriers altogether as early as possible ensures reliability of subsequent operations. To identify them, we use the following heuristic.

$$abs(Var_i(PD)) = \begin{cases} > \tau, & outlier \\ \leq \tau, & \text{otherwise} \end{cases} \tag{8}$$

where $Var_i(PD)$ denotes the variance of the phase difference for the sub-carrier i; The default value for τ is 0.8π.

In the final step of the preprocessing, the Savitzky-Golay polynomial least squares filter (SG Filter) is employed. It serves the purpose of smoothing the signal while preserving the steep changes [23] and is useful for preserving the position of the peaks and valleys. Fig. 8(f) shows an example of pre-processed single sub-carrier.

3.3.3. Selecting sub-carriers

While previous work exists on selecting the informative sub-carriers [15,16], we base our sub-carrier selection algorithm on an observation that sub-carriers with high variance are more representative of the actual breathing pattern. Fig. 9 shows the correlation matrix of all 30 sub-carriers (each scaled to [0–1]) sorted by their variance. We include the reference signal ("GT") in the calculation. We observe: 1) high variance of sub-carrier signals correlates strongly with GT, 2) top sub-carriers correlate well with each other. Based on these observations, we select sub-carrier that has the highest variance and passes certain criteria and then select all other sub-carriers that correlate well with it. These selected sub-carriers will be fused later by the waveform estimation module. The detailed selection procedure is as follows:

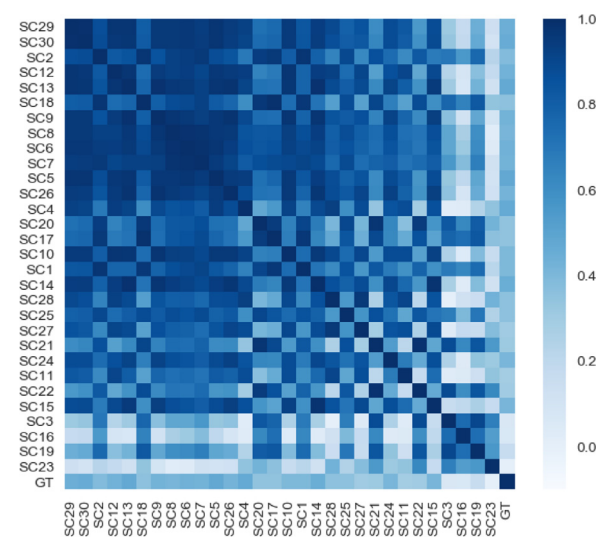

Fig. 9. Sub-carriers Correlation : shows the correlation between all sub-carriers and the ground truth (GT) for a subject breathing normally. Matrix rows are ordered by their variance, the highest value on the top. Sub-carriers with higher variance show a better correlation with GT in general.

- We sort sub-carriers in descending order based on their variance.
- For the top 20 sub-carriers, we calculate the *correlation score* as the average correlation between it and every other sub-carrier in this list.
- We pick the sub-carrier with highest *correlation score* as the *reference* if its number of peaks is close to the median number of peaks for all top sub-carriers (less than one standard deviation). Otherwise, it will be discarded and the next candidate will be considered. The rationale is based on the observation that sub-carrier's high variance does not necessarily reflect its sensitivity level. A noisy sub-carrier with high variance will have a much higher number of peaks than the majority of other sub-carriers due to random fluctuations.
- The process is continued until a suitable reference sub-carrier is found.

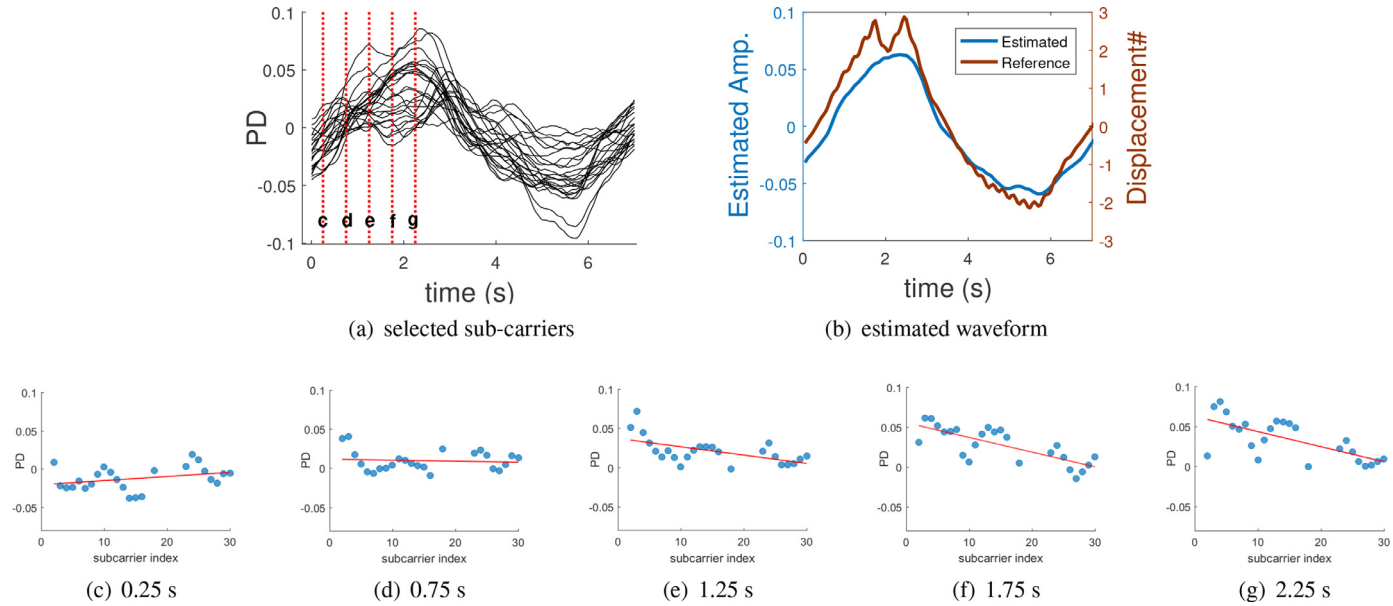

(a) selected sub-carriers (b) estimated waveform

(c) 0.25 s (d) 0.75 s (e) 1.25 s (f) 1.75 s (g) 2.25 s

Fig. 10. Breathing Waveform Estimation as explained by Eq. (7) by regressing over successive PD samples (c-g samples in (a)). Based on this the estimated waveform aligns well with ground truth (b).

- From all sub-carriers, we add the sub-carriers that are strongly correlated with the reference one (absolute correlation ≥ 0.65) to the list.

3.3.4. Alignment

Some sub-carriers in the selected subset will have an opposite phase to the reference sub-carrier. We align all sub-carriers with the reference one by inverting sub-carriers that have negative cross-correlation with the reference signal.

3.3.5. Estimating breathing waveform

The input to this step is a number of PD streams (or time series) where each stream corresponds to a selected de-noised and aligned sub-carrier. The black curves in Fig. 10 show an example. In this step, we 'average' these data streams to compute the relative displacement via linear estimation.

Linear Estimation. The rationale behind linear estimation is related to our earlier observation that the phase difference and chest displacement are linearly related. The idea is that, at each time instance, we perform a linear regression with the PD of the sub-carriers as the dependent variables and the inverse wavelength of the sub-carriers $\frac{1}{\lambda_i}$ as the regressors. To illustrate this idea, we selected five time instances which are indicated by the red dotted lines in Fig. 10(1). At each time instance, we plot the PD of the selected sub-carrier against the sub-carrier index in sub-figures (c)–(g) in Fig. 10. These sub-figures also show the fitted line in red color. We can see from these figures that the trend is almost linear but the noise level is fairly high. By repeating this process for all time instances, we arrive at the estimated relative displacement. Fig. 10(b) compares the estimated relative displacement (calibration information utilized) and the ground truth. To counter the error that might result from fusing noisy sub-carriers, the regression residual error is continually monitored for every selected sub-carrier and the overall median as well. When the residual error of specific sub-carrier is higher than the median by more than 1.5 standard deviation, it will be excluded and the regression-based estimation will be repeated to produce a refined estimation.

Fig. 11 (a) shows example estimated waveform during normal breathing session and the corresponding reference waveform. In this example, WiRelax achieves timing error of 0.21 s (12.2% relative timing error). The inhalation to exhalation ratio (I/E ratio) is another metric commonly used in paced breathing exercises and WiRelax estimates it with an error of 14.4%. Visually, we can observe the similarity between the estimated and the reference waveforms across the five-minute segment and this is confirmed by the high correlation (0.88) and low RMSE (0.12) of the reconstructed wave-form and the reference signal. Fig. 12 shows correlation between the estimated and the reference waveforms for various respiratory pattern examples.

4. Evaluation

4.1. Goals, metrics and methodology

We show that WiRelax provides real-time *full-cycle* respiration feedback during meditation practice. For this purpose, we consider a meditation space, also called "Quiet Room". Similar rooms are available to employees in work environments [24]. The subject would place her portable WiFi enabled devices in front of her, pick a specific exercise (or manually setting inhalation/exhalation time), and start practicing. Feedback is provided during the session. We employ a pair of laptops as the communicating devices[3]. Typically, the user would need the devices close enough to be able to observe the real-time feedback. Nevertheless, in our experiments, we vary the distances in the range 1–3 m to evaluate the performance of WiRelax for different room sizes.

Feedback: Although we leave the feature-rich interactive user interface design as a future work, we designed an initial prototype for providing in-session feedback (Fig. 13). After experimenting with a few designs, we find the circular segmented (radial donut) user interface component is generally preferred by the subjects (top left in Fig. 13). We process incoming packets every 0.1 s to simulate real-time input. WiRelax processing was implemented on MacBook Pro-running macOS Sierra v 10.12.6 with 8 GB RAM and 2.7 GHz Intel Core i5 processor. Implementation was done in Python 3. NumPy and scikit-learn libraries were utilized for pro-

[3] Currently, commodity smartphones' wireless cards can export CSI data using tools as Nexmon Channel State Information Extractor (https://github.com/seemoo-lab/nexmon_csi)

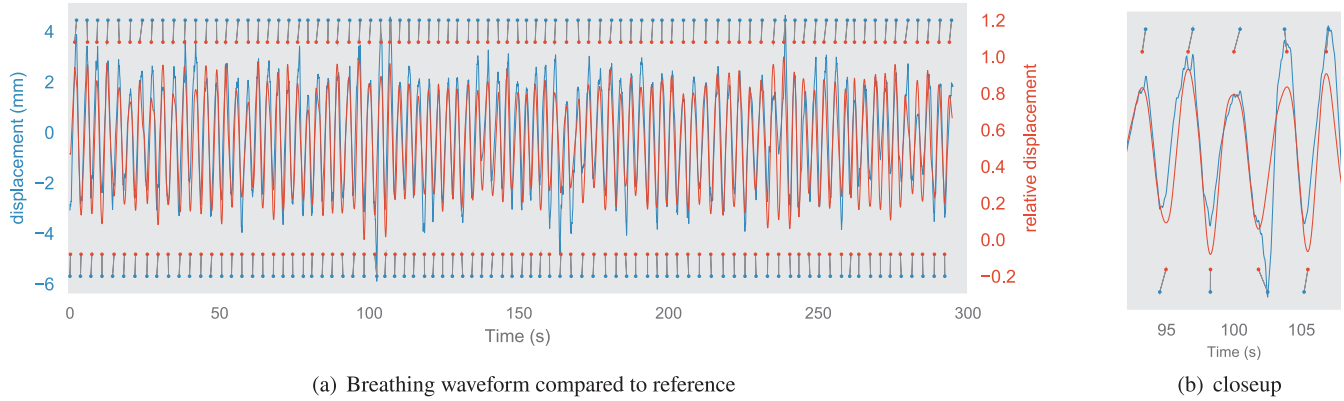

(a) Breathing waveform compared to reference (b) closeup

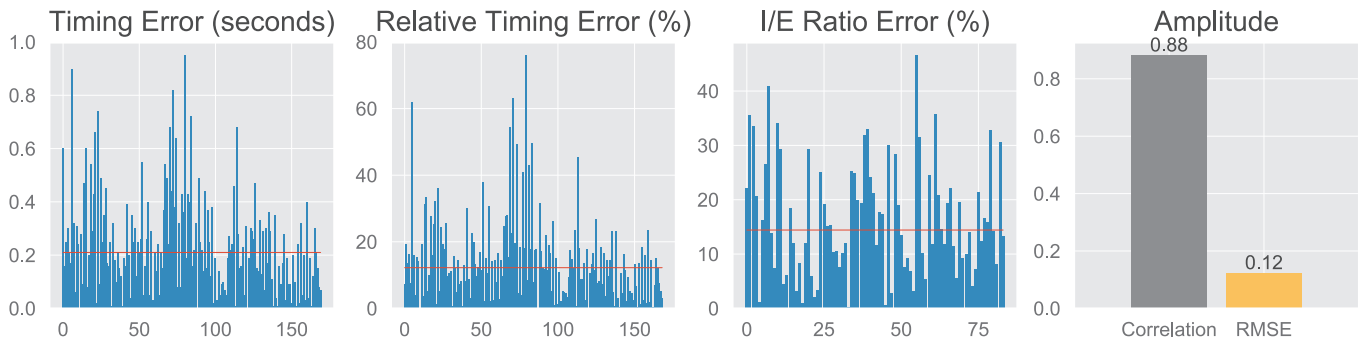

(c) Error

Fig. 11. Breath cycles tracking for a segment of normal breathing session. (a) estimated relative displacement waveform compared to reference displacement waveform. Peaks and valleys positions are visualized on top and bottom, respectively, slanting lines signify the deviation direction [as shown in the closeup (b)]. (c) breath tracking accuracy for various metrics. The red lines denote the medians: 0.21 s, 12.2% and 14.4% for cycle timing error, relative timing error and I/E ratio error respectively. The correlation and root mean squared error between the estimated waveform and reference signal are also reported. (For interpretation of the references to colour in this figure legend, the reader is referred to the web version of this article.)

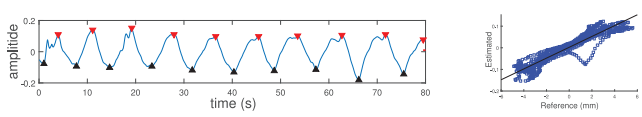

(a) rate: 8 bpm, chest displacement var: 6.2 mm (b)

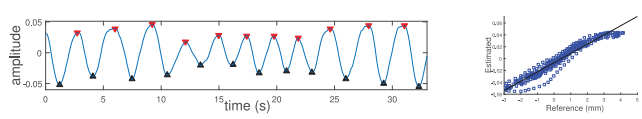

(c) rate: 21 bpm , chest displacement var: 4.4 mm (d)

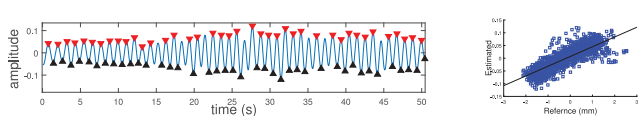

(e) rate: 45 bpm , chest displacement var: 1.07 mm (f)

Fig. 12. (a), (c) and (e) estimated waveforms for deep breathing, deep & normal breathing and quick breathing sessions, respectively. (b), (d) and (f) show scatter plots of estimated relative displacement against the true displacement.

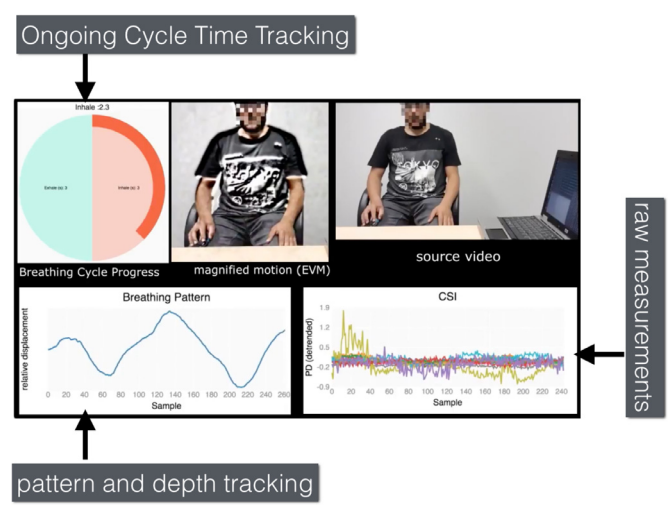

Fig. 13. WiRelax biofeedback prototype (demo: https://youtu.be/e_er2w39b4I).

cessing data and rendering the output. With these configurations, it takes WiRelax 180 ms on average to process one second of input data and produce the estimated waveform.

Data Collection We collected data from several "quiet rooms" to evaluate WiRelax. The WiFi transmitter and receiver are HP elitebook 6930p Laptops equipped with Intel 5300 WiFi cards. These laptops are placed on a desk and collect the WiFi CSI data using Linux 802.11n CSI Tool [25]. The ground truth for chest displacement was collected by an X2-M200 UWB-IR sensor [26]. This sensor has been employed in a variety of vital sign monitoring applications [26] and reportedly has a maximum deviation of 5% compared to PSG reference airflow and thorax/abdomen displacement measurements [27]. The sensor reports chest displacement in millimeters at 20Hz sampling rate. Ten volunteers (8 males and

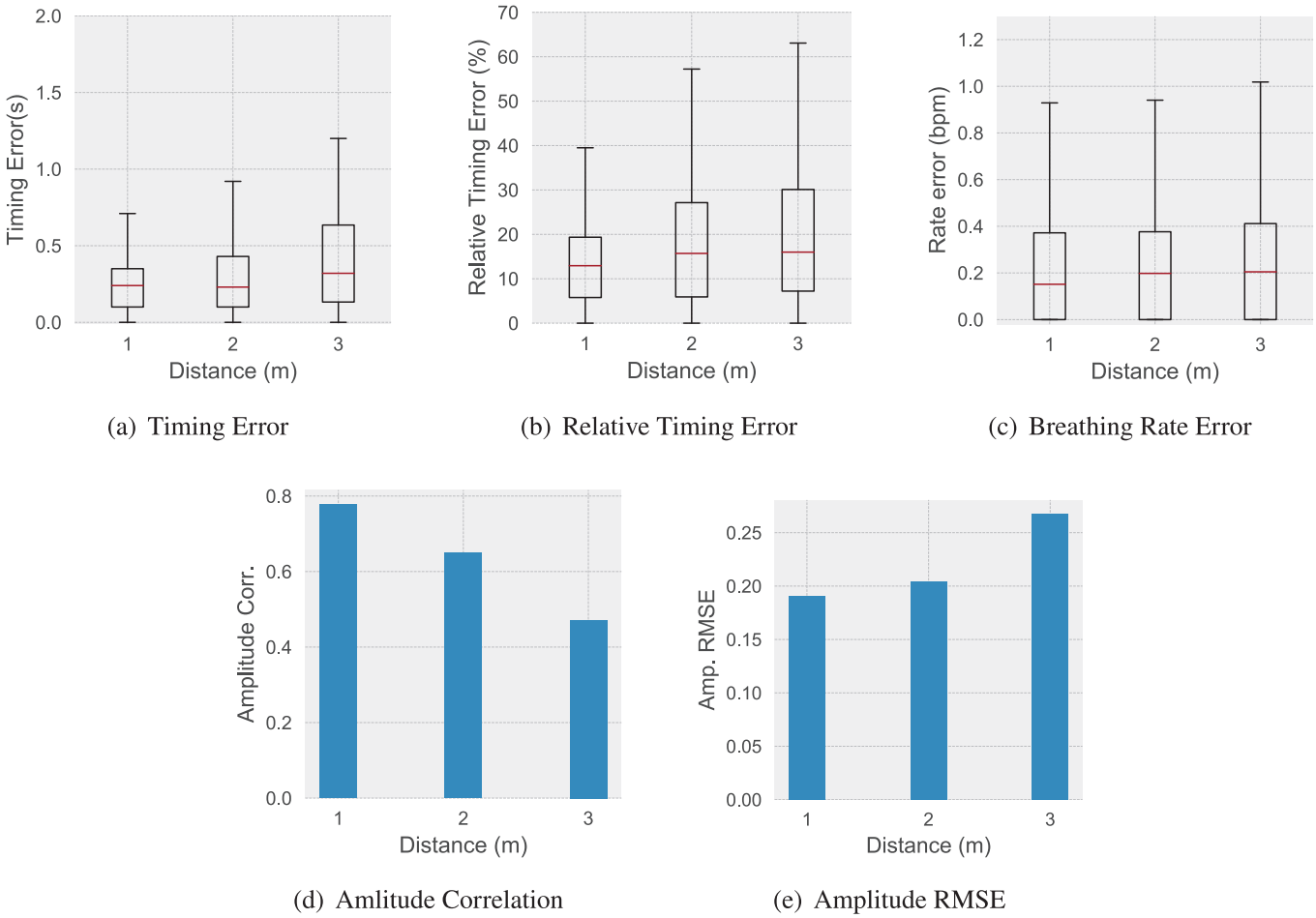

(a) Timing Error (b) Relative Timing Error (c) Breathing Rate Error

(d) Amlitude Correlation (e) Amplitude RMSE

Fig. 14. Evaluation of different breathing accuracy metrics with respect to distance between the user and WiRelax system.

2 females) participated in the data collection process over a total period of 4 months.[4] For each user, we run several experiments to evaluate the impact of the distance between the user and the sensor on WiRelax algorithm performance. We select the key signal processing parameters using leave-one-out cross validation (LOOCV) in which data from single user is used for testing the parameters that were determined using data from all other users.

Metrics: We use the same quantitative metrics as previous work, including the real-time cycle timing error and relative timing error (also called progress time error) metrics used by Hao et al. [7], and the normalized amplitude Root Mean Squared Error (RMSE) and correlation between normalized waveforms used by Lee et al. [28].

4.2. Capturing breathing cycles

In this section we evaluate the performance of WiRelax in terms of the accuracy of breathing cycle time and amplitude estimation. We also study the impact of the distance parameter h defined in Section 3.2. Fig. 14 shows the accuracy of the proposed system for various timing and amplitude related metrics across the three distances considered.

Fig. 14 (c) plots the breathing rate error. The system estimates the rate accurately, with a median error of 0.15 bpm for a distance of 1 m, which slightly increases to 0.2 bpm for larger distances. Inhalation and exhalation cycles are also captured accurately (see Fig. 14(a)) with median errors of 0.24 s, 0.23 s and 0.32 s for 1 m, 2 m and 3 m, respectively. We note that an error in the cycle time estimation has a direct impact on the next cycle. For example, a small positive error in the inhalation cycle of +0.1 s will introduce an error of −0.1 s in the following exhalation cycle.

The relative timing error is a more descriptive measurement of the timing accuracy because the cycle length is taken into account here. WiRelax achieves the median relative timing error of 12.9% at a 1 m distance. Intuitively, the timing errors observed in WiRelax are related to the number and the quality of representative subcarrier signals measured by the Wi-Fi hardware. Signal-to-noise ratio of these signals decreases with increasing *distance* between the test subject and the measurement apparatus, which translates into lower accuracy.

Amplitude-related metrics are shown in Fig. 14(d), (e). Similar to the timing metrics, amplitude estimation performance degrades with an increasing distance, albeit at a higher rate. There are two reasons for this. First, timing-based metrics are only impacted by the cycle start/end positions while amplitude is impacted by the whole PD time-series that dictate the waveform shape. Second, misalignment caused by the timing errors further amplifies the amplitude errors.

4.3. Capturing complete breathing pattern

While WiRelax is concerned mainly with providing accurate in-session feedback to the user, it is informative to put WiRelax in

[4] Data collection approved by Human Research Ethics committee in University of New South Wales.

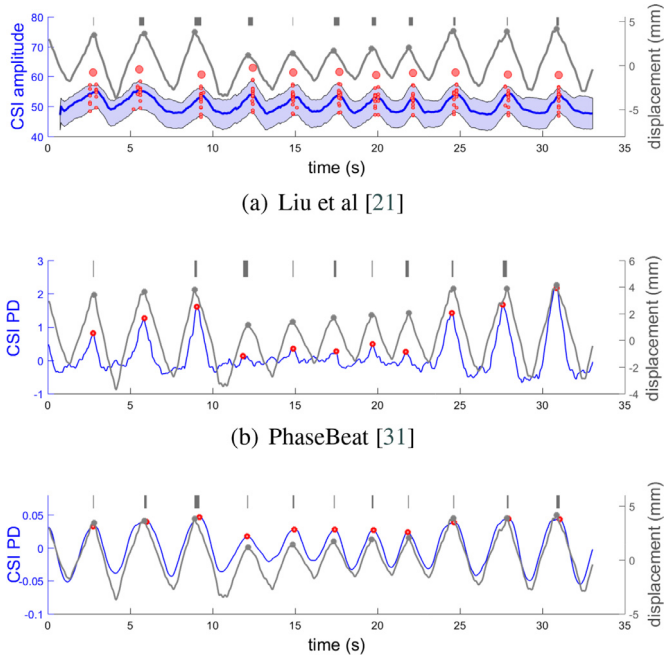

Fig. 15. This plot shows the results of breathing cycle estimations from three algorithms: Liu et al. [16], PhaseBeat and WiRelax. The gray line shows the ground truth for chest displacement. The solid gray (red) circles show the true (estimated) peak. The ticks show the time difference between the estimated and true peak (i.e. the difference in timings of the red and gray circles). (a) Liu et al. [16] estimates cycle period using all peaks (small red circles) of selected sub-carriers. The weighted average of all sub-carriers cycle time determines the final breathing cycle boundaries (marked by large red circles). (b) PhaseBeat [18] employs inter-peak duration for a chosen single sub-carrier to estimate the breathing rate. (c) **WiRelax** employs a cohort of selected sub-carriers to estimate the final breathing waveform. (For interpretation of the references to colour in this figure legend, the reader is referred to the web version of this article.)

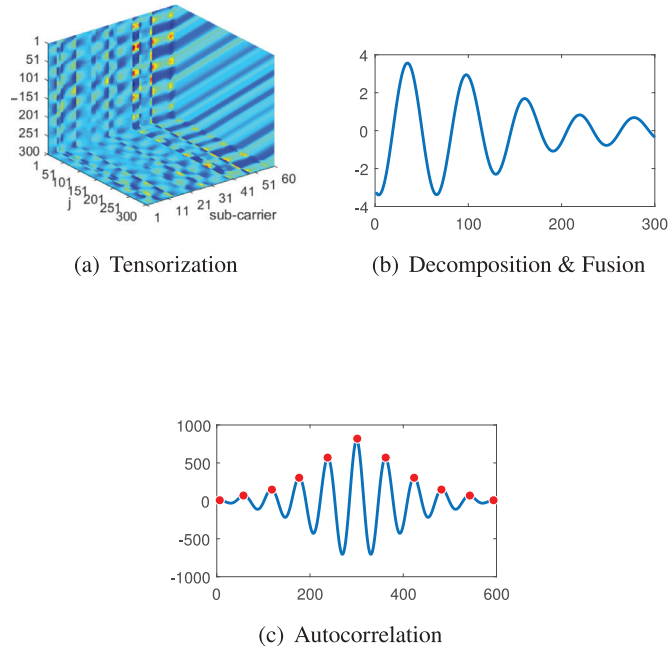

Fig. 16. TensorBeat [29] processing for same data of Fig. 15.

context with state-of-the-art WiFi-based breathing monitoring systems. We focus on amplitude-based system [16] and two phase difference-based systems [18] and [29]. For objective comparison we consider only the breathing rate for [29] and the complete cycle length metric for [16], while the complete waveform (timing and waveform amplitude) is compared to PhaseBeat [18].

We present brief description of these systems along with replication considerations for convenience:

- Liu et al. [16]: amplitude measurements from 30 sub-carriers are used. Data calibration is applied to mitigate the noise in raw data. Then, the most sensitive sub-carriers (blue curve area in Fig. 15(a)) are selected based on their variance. Next, peaks locations are calculated while considering fake peak removal in the process. Finally, weighted average of all peak-to-peak intervals across selected sub-carriers is employed to get the breathing rate.
- PhaseBeat [18]:Phase difference data from 30 sub-carriers at 400 Hz sampling rate are used as input. DC component and high frequency noises are removed through calibration. Next, the top 3 sub-carriers with maximum mean absolute deviations are picked. Out of them, the median one is the final selection.
- TensorBeat [29]:
  Phase difference data from 60 sub-carriers (two antenna pairs) at 20 Hz sampling rate are used as input. After calibration, a two-dimensional Hankel matrix is constructed from 600 consecutive packets of each sub-carriers. The 60 Hankel matrices are stacked into the 3-dimensional tensor. Since we have a single user, the tensor's rank was fixed to 2. Next, tensor decomposition is applied using CP decomposition [30] and autocorrelation is calculated on the fusion of the decomposed signal pairs. Finally, the rate is reported based on average inter-peak duration.

We show the performance of different algorithms based on an experiment with one subject. Over a period of 30 s, the subject was asked to perform deep breathing for 10 s, then normal breathing for 10 s and finally deep breathing for 10 s. The purpose is to create a breathing pattern whose amplitude varies over time. The true breathing pattern captured by the UWB sensor is plotted in gray line in Fig. 15(a)–(c).

The WiFi CSI data was processed by the algorithm of Liu et al., as well as PhaseBeat, WiRelax and TensorBeat. The results from the three algorithms are shown in Fig. 15(a)–(c) while those for TensorBeat are in Fig. 16.

We first consider Fig. 15(a)–(c). In these figures, the solid gray and red circles show the timing of the true and estimated peaks, respectively. The gray ticks near the top of each subplot show the deviation between the timing of the true and estimated peaks. Therefore, a wider tick indicates a larger timing error and vice versa.

For waveform estimation, it can readily be seen that WiRelax has the least timing error, 0.21 s compared to 0.41 s and 0.266 s for Liu et al. [16] and PhaseBeat. In addition, WiRelax is able to get the relative chest displacement amplitude much more accurately compared to PhaseBeat (WiRelax Normalized RMSE is 0.1081 compared to 0.2716 by PhaseBeat). TensorBeat estimates the breathing rate from the median peak-to-peak distances (see Fig. 16(c)). The fused breathing signal 16(b) doesn't match the actual breathing pattern. While a noticeable decrease in breathing depth can be seen in Fig. 16(b), the state transition (deep to shallow to deep again) is missing.

5. Related work

The work presented here is related to the relatively large body of literature about respiration tracking. In this section we survey several categories of research and the related consumer products available in the market.

In a clinical setting, Respiratory Inductance Plethysmography (RIP) [31,32] is commonly used as the "gold standard" for monitoring respiration. Although it is accurate, the cost and inconvenience of RIP motivates researchers to investigate alternative techniques, especially for applications that require daily monitoring. The techniques generally break down to two categories: wearable device and device-free monitoring.

5.1. Wearable device monitoring

A large body of previous research used attachable sensors to monitor breathing. Examples include, textile-based systems [5,6] that imitate RIP by using conductive materials that track the expansion and contraction of chest during respiration. Zephyr [33] used built-in accelerometer and gyroscope sensors in a phone placed on the user's chest to estimate respiratory rate. Recently, MindfulWatch [7] proposed the use of smartwatch's inertial sensors to track breathing cycles in real-time for meditation applications.

Stress detection and management based on breathing monitoring is also a commercially active area. For example, Spire [8] uses a patented respiration sensor [34] to collect respiration characteristics and recommends meditation sessions and breathing exercises to manage the stress. Prana [9] monitors breathing patterns using wearable pod or belt and offers interactive games (controlled through breathing) for guiding the users during breathing exercises.

5.2. Device-free monitoring

Closely related to our approach, device free systems can monitor vital signals of a user without requiring the user to wear a sensor. Among them, RF based sensing systems belong to the most popular device-free systems.

Respiration Rate Sensing: UbiBreathe [17] employs WiFi radio signal strength (RSS) to monitor breathing rates. mmVital uses RSS of a 60 GHz millimeter wave signal for breathing and heart rates monitoring. Liu et al. [16] and PhaseBeat [18] leveraged WiFi channel state information (CSI) to monitor breathing rate and, also, heart rate after utilizing directional antennas. Later, CardioFi [35] leveraged enhanced sub-carrier selection mechanism for better heart rate monitoring without requiring special antennas. A number of amplitude-based respiration sensing systems [15,20] based on the Fresnel Zone Model were developed. The model relates one's chest movement to the received WiFi signals amplitude measurements. As chest displacement crosses Fresnel zones, the receiving signal shows a continuous sinusoidal-like wave, with peaks and valleys generated by crossing the boundaries. This allows for breathing pattern extraction. Our model, on the other hand, is based on the phase difference measurements and goes beyond pattern capturing to explain how breathing depth can impact captured PD measurements.

Respiration Detection Range: Recently, there are a few works focused on improving the detection range of WiFi breathing. Fullbreath [36] uses phase and amplitude measurements simultaneously and employs conjugate multiplication of two antenna measurements to improve breathing detectability. FarSense [37] proposed to use "CSI ratio" to push the respiration sensing range to house level (up to 8–9 m).

The main distinction between our work and related device-free WiFi breathing monitoring systems is the focus on extracting breathing biofeedback information. For this, our system is designed to address the requirements of reporting instantaneous breathing depth and timing while the breathing cycle is still ongoing. The ability of the proposed model to regress directly on incoming PD measurements enables such tracking without having to wait for the cycle completion. This, in turn, enables WiFi-based interactive breathing applications.

6. Limitations and future work

Advances in device-free sensing using COTS WiFi have recently sparked a renewed interest in their applications for fine-grained sensing applications including vital sign monitoring. In this work we focused on reliable and detailed monitoring of the breath cycle and its characteristics. Our findings suggest that COTS WiFi can be effectively employed for conscious breathing monitoring and real-time feedback.

However, WiRelax has its limitations. First, the CSI data is sensitive to multi-path interference specific to the environmental setup. We acknowledge that WiRelax performance might be impacted by the movement of people nearby. The *environmental impact* limitation is fundamental to WiFi and other device-free sensing systems and presents an important challenge for future research [38]. Currently, we are exploring ways to mitigate the impact of irrelevant motions, for example, by developing a "Breath Model" [7] for the users. Breathing patterns do not change dramatically between consecutive cycles, which allows us to suppress the noise in the breathing cycle estimation by fusing information from a previous (noise-free) reference cycle.

Second, we adopted preliminary visual feedback scheme in the WiRelax prototype, to demonstrate the real-time breath-by-breath monitoring capability. The subject can observe his instantaneous behavior and adapt accordingly. However, a further user-centric study might be needed to improve its responsiveness and make it more intuitive. For example, studies show that auditory feedback is superior to visual feedback in creating self-reported calm [39]. Another important feedback that our system can provide is a summarized per-session breathing performance, which is vital for long-term tracking of breathing habits. Our future work will investigate visual, auditory, and summary features to further improve WiRelax capabilities.

7. Conclusions

To enable interactive breath control applications, this paper proposed contact-less sensing of instantaneous breathing dynamics using WiFi channel (CSI). Tracking on-going breath cycles using WiFi was never explored in past research as per authors' best knowledge. Contrary to complete cycles tracking (breathing rate), on-going cycle progress reporting is complicated by the need to map divergent measurements from noisy sub-carriers into a single instantaneous breathing state (time and depth) while maintaining sub-second responsiveness (i.e. instant sensing and feedback loop) necessary for biofeedback. We approached the problem guided by observations about the stability of phase difference (PD). Our study of the impact of micro-motions on the PD measurements culminated into a model showing the linear relation between the two quantities. Interestingly, this enables mapping the instantly measured PD into chest displacement (up to relative constant). Consequently, inferring breathing progress without waiting cycle completion is theoretically feasible. To get reliable estimation in practice, a novel sub-carrier filtering and selection was adopted and robustness was further enforced by leveraging simple per-session calibration procedure. WiRelax is able to report sub-second breathing progress in real-time with median timing error of 0.25 s. The system requires neither training nor information about subject identity and ready to deploy on off-the-shelf WiFi devices.

This opens the door to employing WiFi sensing in biofeedback applications on large scale.

Declaration of Competing Interest

The authors declare that they have no known competing financial interests or personal relationships that could have appeared to influence the work reported in this paper.

Supplementary material

Supplementary material associated with this article can be found, in the online version, at doi:10.1016/j.adhoc.2020.102226.

References

[1] K. Plarre, A. Raij, S.M. Hossain, A.A. Ali, M. Nakajima, M. Al'absi, E. Ertin, T. Kamarck, S. Kumar, M. Scott, et al., Continuous inference of psychological stress from sensory measurements collected in the natural environment, in: 2011 10th International Conference on Information Processing in Sensor Networks (IPSN), IEEE, 2011, pp. 97–108.

[2] K.D. Chandwani, B. Thornton, G.H. Perkins, B. Arun, N. Raghuram, H. Nagendra, Q. Wei, L. Cohen, Yoga improves quality of life and benefit finding in women undergoing radiotherapy for breast cancer., J. Soc. Integr. Oncol. 8 (2) (2010).

[3] A.E. Holland, C. Hill, A. Jones, C. McDonald, Breathing exercises for chronic obstructive pulmonary disease, Cochrane Database Syst. Rev. 10 (2010).

[4] E. Holloway, F. Ram, Breathing exercises for asthma, Cochrane Database Syst. Rev. 1 (2004).

[5] L. Guo, L. Berglin, Y. Li, H. Mattila, A.K. Mehrjerdi, M. Skrifvars, 'Disappearing Sensor'-textile based sensor for monitoring breathing, in: Control, Automation and Systems Engineering (CASE), 2011 International Conference on, IEEE, 2011, pp. 1–4.

[6] E. Mitchell, S. Coyle, N.E. O'Connor, D. Diamond, T. Ward, Breathing feedback system with wearable textile sensors, in: Body Sensor Networks (BSN), 2010 International Conference on, IEEE, 2010, pp. 56–61.

[7] T. Hao, C. Bi, G. Xing, R. Chan, L. Tu, MindfulWatch: a smartwatch-based system for real-time respiration monitoring during meditation, Proc. ACM Interact. Mob.Wearable Ubiquitous Technol. 1 (3) (2017) 57.

[8] Spire, 2018a, URL: https://spire.io/.

[9] Prana, 2018b, URL: http://www.prana.co.

[10] Apple breathe app, 2018c, URL: https://support.apple.com/en-ke/HT206999.

[11] Witherapy demo, 2018d, URL: https://youtu.be/e_er2w39b4I.

[12] F. Adib, H. Mao, Z. Kabelac, D. Katabi, R.C. Miller, Smart homes that monitor breathing and heart rate, in: Proceedings of the 33rd Annual ACM Conference on Human Factors in Computing Systems, ACM, 2015, pp. 837–846.

[13] R. Ravichandran, E. Saba, K.-Y. Chen, M. Goel, S. Gupta, S.N. Patel, WiBreathe: estimating respiration rate using wireless signals in natural settings in the home, in: Pervasive Computing and Communications (PerCom), 2015 IEEE International Conference on, IEEE, 2015, pp. 131–139.

[14] M. Nowogrodzki, D. Mawhinney, H. Milgazo, Non-invasive microwave instruments for the measurement of respiration and heart rates, NAECON 1984 1984 (1984) 958–960.

[15] H. Wang, D. Zhang, J. Ma, Y. Wang, Y. Wang, D. Wu, T. Gu, B. Xie, Human respiration detection with commodity WiFi devices: do user location and body orientation matter? in: Proceedings of the 2016 ACM International Joint Conference on Pervasive and Ubiquitous Computing, ACM, 2016, pp. 25–36.

[16] J. Liu, Y. Wang, Y. Chen, J. Yang, X. Chen, J. Cheng, Tracking vital signs during sleep leveraging off-the-shelf WiFi, in: Proceedings of the 16th ACM International Symposium on Mobile Ad Hoc Networking and Computing, ACM, 2015, pp. 267–276.

[17] H. Abdelnasser, K.A. Harras, M. Youssef, UbiBreathe: a ubiquitous non-invasive WiFi-based breathing estimator, in: Proceedings of the 16th ACM International Symposium on Mobile Ad Hoc Networking and Computing, ACM, 2015, pp. 277–286.

[18] X. Wang, C. Yang, S. Mao, PhaseBeat: exploiting CSI phase data for vital sign monitoring with commodity WiFi devices, in: Distributed Computing Systems (ICDCS), 2017 IEEE 37th International Conference on, IEEE, 2017, pp. 1230–1239.

[19] I. Van Diest, K. Verstappen, A.E. Aubert, D. Widjaja, D. Vansteenwegen, E. Vlemincx, Inhalation/exhalation ratio modulates the effect of slow breathing on heart rate variability and relaxation, Appl. Psychophysiol. Biofeedback 39 (3–4) (2014) 171–180.

[20] D. Zhang, H. Wang, D. Wu, Toward centimeter-scale human activity sensing with Wi-Fi signals, Computer 50 (1) (2017) 48–57.

[21] W. Wang, A.X. Liu, M. Shahzad, K. Ling, S. Lu, Understanding and modeling of WiFi signal based human activity recognition, in: Proceedings of the 21st Annual International Conference on Mobile Computing and Networking, ACM, 2015, pp. 65–76.

[22] Z. Yang, P.H. Pathak, Y. Zeng, X. Liran, P. Mohapatra, Monitoring vital signs using millimeter wave., in: MobiHoc, 2016, pp. 211–220.

[23] J. Luo, K. Ying, J. Bai, Savitzky–Golay smoothing and differentiation filter for even number data, Signal Process. 85 (7) (2005) 1429–1434.

[24] Corporate meditation: how and why big businesses are promoting meditation, 2018, URL: https://tinyurl.com/yc7hbhyq.

[25] D. Halperin, W. Hu, A. Sheth, D. Wetherall, Tool release: Gathering 802.11 n traces with channel state information, ACM SIGCOMM Computer Communication Review 41 (1) (2011). 53–53

[26] Xethru x2m200, 2018, URL: https://www.xethru.com/respiration-sensor-x2m200.html.

[27] D.T. Wisland, K. Granhaug, J.R. Pleym, N. Andersen, S. Støa, H.A. Hjortland, Remote monitoring of vital signs using a CMOS UWB radar transceiver, in: New Circuits and Systems Conference (NEWCAS), 2016 14th IEEE International, IEEE, 2016, pp. 1–4.

[28] Y.S. Lee, P.N. Pathirana, R.J. Evans, C.L. Steinfort, Noncontact detection and analysis of respiratory function using microwave doppler radar, J. Sens. 2015 (2015).

[29] X. Wang, C. Yang, S. Mao, TensorBeat: tensor decomposition for monitoring multi-person breathing beats with commodity WiFi, arXiv:1702.02046 (2017).

[30] T.G. Kolda, B.W. Bader, Tensor decompositions and applications, SIAM Rev. 51 (3) (2009) 455–500.

[31] P. Grossman, F.H. Wilhelm, M. Brutsche, Accuracy of ventilatory measurement employing ambulatory inductive plethysmography during tasks of everyday life, Biol. Psychol. 84 (1) (2010) 121–128.

[32] J.D. Witt, J.R. Fisher, J.A. Guenette, K.A. Cheong, B.J. Wilson, A.W. Sheel, Measurement of exercise ventilation by a portable respiratory inductive plethysmograph, Respir. Physiol. Neurobiol. 154 (3) (2006) 389–395.

[33] H. Aly, M. Youssef, Zephyr: Ubiquitous accurate multi-sensor fusion-based respiratory rate estimation using smartphones, in: Computer Communications, IEEE INFOCOM 2016-The 35th Annual IEEE International Conference on, IEEE, 2016, pp. 1–9.

[34] J. PALLEY, Z. ZHAO, System and method for monitoring respiration, 2014.

[35] A. Khamis, C.T. Chou, B. Kusy, W. Hu, CardioFi: Enabling heart rate monitoring on unmodified cots WiFi devices, in: Proc. EAI 15th Int. Conf. Mobile Ubiquitous Syst., Comput., Netw. Services (Mobiquitous), 2018.

[36] Y. Zeng, D. Wu, R. Gao, T. Gu, D. Zhang, FullBreathe: full human respiration detection exploiting complementarity of CSI phase and amplitude of WiFi signals, Proc. ACM Interact. Mob.Wearable Ubiquitous Technol. 2 (3) (2018) 148.

[37] Y. Zeng, D. Wu, J. Xiong, E. Yi, R. Gao, D. Zhang, FarSense: pushing the range limit of WiFi-based respiration sensing with CSI ratio of two antennas, arXiv:1907.03994 (2019).

[38] W. Jiang, C. Miao, F. Ma, S. Yao, Y. Wang, Y. Yuan, H. Xue, C. Song, X. Ma, D. Koutsonikolas, W. Xu, L. Su, D. Kout, Towards environment independent device free human activity recognition, in: Proceedings of the 21st Annual International Conference on Mobile Computing and Networking, ACM, 2018.

[39] K. Wongsuphasawat, A. Gamburg, N. Moraveji, You can't force calm: designing and evaluating respiratory regulating interfaces for calming technology, in: Adjunct Proceedings of the 25th Annual ACM Symposium on User interface Software and Technology, ACM, 2012, pp. 69–70.

Abdelwahed Khamis is a Research Associate at the School of Computer Science and Engineering, UNSW, Sydney and a Visiting Scientist in Data61, CSIRO. He has a PhD degree in Computer Science and Engineering from UNSW, Australia and Bsc and Msc in Computer Science from Zagazig University, Egypt. His Ph.D. research focused on the use of RF technologies for medical sensing applications including Hand Hygiene tracking and vital sign monitoring His research interests include ubiquitous and device-free sensing, mobile computing and wireless security.

Brano Kusy is a principal research scientist in CSIRO and the leader of the Pervasive Computing team. He has a Ph.D. degree in Computer Science from Vanderbilt University, Nashville, USA and an MS degree in Computer Science from Comenius University, Bratislava, Slovakia. His Ph.D. work was on embedded wireless sensor systems, applied in various application scenarios, including acoustic sniper localization and low-power wireless localization and tracking. His main research focus was on system services that enable time and space coordination in embedded distributed systems.

Chun Tung Chou received the B.A. degree in engineering science from the University of Oxford, U.K., and the Ph.D. degree in control engineering from the University of Cambridge, U.K. He is currently an Associate Professor with the School of Computer Science and Engineering, University of New South Wales, Australia. His research interests are in molecular communication, molecular computing, and pervasive computing. He is on the Editorial Board of the IEEE Transactions on Molecular, Biological, and Multi-Scale Communications, IEEE Wireless Communications Letters, and Nano Communication Networks.

Wen Hu is an associate professor at School of Computer Science and Engineering, the University of New South Wales (UNSW). Much of his research career has focused on the novel applications, low-power communications, security and compressive sensing in sensor network systems and Internet of Things (IoT). Hu published regularly in the top rated sensor network and mobile computing venues such as ACM/IEEE IPSN, ACM SenSys, ACM MobiCOM, ACM UbiCOMP, IEEE PerCOM, ACM transactions on Sensor Networks (TOSN), IEEE Transactions on Mobile Computing (TMC), and Proceedings of the IEEE. Hu was a principal research scientist and research project leader at CSIRO Digital Productivity Flagship, and received his Ph.D from the UNSW. He is a recipient of prestigious CSIRO Office of Chief Executive (OCE) Julius Career Award (2012 - 2015) and multiple research grants from Australian Research Council, CSIRO and industries. Hu is a senior member of ACM and IEEE, and is an associate editor of ACM TOSN and the general chair of CPS-IoT Week 2020, as well as serves on the organising and program committees of networking conferences including ACM/IEEE IPSN, ACM SenSys, ACM MobiCOM, ACM MobiSys, ACM/IEEE IOTDI, IEEE ICDCS. Hu works as the Chief Scientist (part time) in WBS Tech to commercialise his research results in smart buildings and IoT since 2017.